Conformations of Flexible Dendrimers: A Simulation Study

I. O. Götze[†] and C. N. Likos*[,†,‡]

Institut für Theoretische Physik II, Heinrich-Heine-Universität Düsseldorf, Universitätsstrasse 1, D-40225 Düsseldorf, Germany, and University Chemical Laboratory, Lensfield Road, Cambridge CB2 1EW, United Kingdom

Received February 24, 2003; Revised Manuscript Received July 28, 2003

ABSTRACT: We examine the sizes and conformations of flexible dendrimers of generation numbers $G = 4$ to $G = 9$ by means of Monte Carlo simulations on a coarse-grained level. To this end, we introduce a simple, "bead−thread" model with variable thread-to-bead size ratio δ. In addition, we compare the results from this model to previously calculated ones, based on a soft-sphere−spring model, to test the dependence of the results on the microscopic details. We find a clear insensitivity of the resulting conformational properties on those, both models leading to dense-core density profiles and to increasingly compact structures upon increase of the terminal generation. Moreover, we calculate the distribution of the end monomers, which turns out to be broad and extending throughout the volume occupied by the dendrimer. The dependence of the radius of gyration R_g on the monomer number N does not follow the scaling law $R_g \sim N^{1/3}$ that has been often put forward in the literature, but rather it obeys, for high generation numbers, a dependence of the form $R_g \sim N^{0.24}$.

I. Introduction

Dendrimers are synthetic macromolecules with a treelike, branched structure.[1] Figure 1 shows the architecture of a typical dendritic molecule. In the synthesis of dendrimers, a stepwise iterative reaction is employed: two trifunctional units bonded together form the core or the zeroth generation of the molecule, $g = 0$. Thereafter, monomer chains consisting of P segments each are attached on every functional unit. At its end, the chain branches out to two tips, and on each one of those a new *dendron* grows, the Greek word for *tree* that gives dendrimers their name. The ends of the P-segment chains form the new generation, and the procedure is iterated until a terminal generation G. Thus, it is convenient to denote dendrimers as Gn, where n is a positive integer denoting the final generation number. The length of the intermediate chains, P, is referred to as the spacer length of the dendrimers. In principle, the functionality f of the branching units can also be changed, but most of the studies to date focus on the usual case of trifunctional units, $f = 3$.

Research on dendrimers is a part of modern nanoscience with the aim of tailoring material properties at the molecular level. The motivation for the current investigations rests on the enormous flexibility in modifying the architecture of the dendrimers, in line with the general scheme sketched above, which leads to the possibility of adapting dendrimers to meet various needs in applications.[2] The two-dimensional rendition of the dendrimer's shape shown in Figure 1 suggests a structure with internal voids and with a dense shell and has thus led to the concept of the hollow "dendritic box" that can be employed as carrier for smaller molecules encapsulated in its interior.[3] This dense-shell or hollow-core model of dendrimers was also put forward in the early theoretical analysis of de Gennes and Hervet[4] that was based on self-consistent-field (SCF) calculations. Following the pioneering work of Lescanec and Muthukumar,[5] however, it has been demonstrated in various simulational studies during the past 10 years that the dense-shell model does not describe the conformations of self-avoiding, neutral dendrimers, as we discuss in more detail below. The pitfall in the SCF calculations of de Gennes and Hervet has been their implicit assumption that the end groups of the dendrimers are localized on their periphery. When this restriction is relaxed, then the improved SCF calculations lead to the opposite, dense-core picture of the dendrimers, in which the monomer density monotonically decays with the distance from their center and the end monomers are distributed throughout the molecule. The pioneering theoretical study that led to the dense-core model has been carried out by Boris and Rubinstein.[6] Zook and

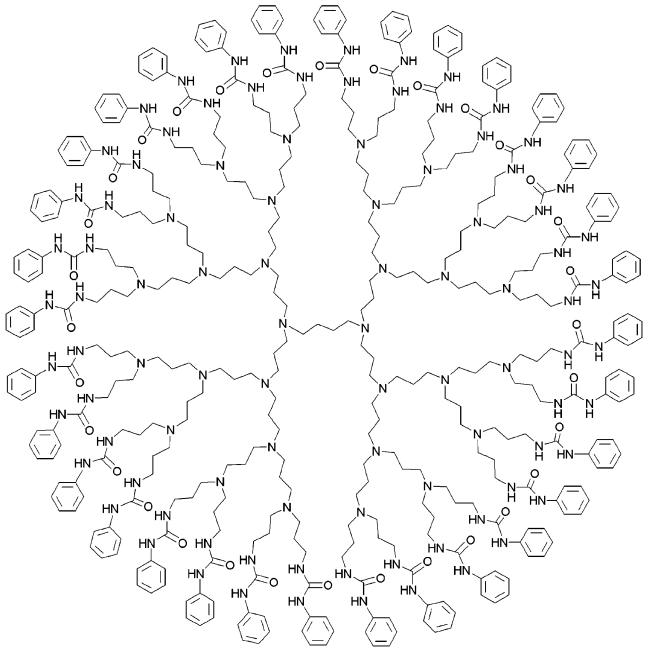

Figure 1. Chemical structure of a dendrimer of fourth generation (courtesy of Matthias Ballauff).

[†] Heinrich-Heine-Universität Düsseldorf.
[‡] University Chemical Laboratory.

10.1021/ma030137k CCC: $25.00
Published on Web 09/18/2003

Pickett[7] have recently revisited the arguments of de Gennes and Hervet and pointed out the weakness that led to the erroneous, dense-shell prediction. The problem lies in the assumption that there is a unique, typical trajectory of a chain that dominates all others, equivalently, a unique "ground state" of the system. However, it turns out that there are infinitely many degenerate trajectories for the self-consistent potential, in analogy to the well-known case of the parabolic, planar polymer brush.[8] When the degeneracy is taken into account, one obtains a parabolic density profile with a maximum at the core as well as a distribution of the chain tips throughout the dendrimer.[7]

Various different models for dendrimers have been proposed in simulation studies of the same, ranging from atomistic ones,[9−12] in which detailed force fields are employed, to coarse-grained ones,[13−22] in which the steric and bonding interactions are modeled by means of simple, radially symmetric pair potentials. Often the simulations of coarse-grained models require specially designed algorithms, such as pivot moves.[15,16] Also, some of the simulations are performed on lattice models, and there special care has to be taken in order to employ moving algorithms that satisfy detailed balance.[13,23−25] It is desirable, thus, to develop an off-lattice model, so that an artificial discretization of space can be avoided, which at the same time is simple enough to be simulated by standard techniques and also sufficiently realistic to capture the salient features of the dendrimers' behavior at the mesoscopic length scale.

In this paper, we introduce a model for dendrimers that is particularly well-suited for performing Monte Carlo (MC) simulations. Because of its simplicity, it allows for a systematic investigation of the dendrimers' properties for a wide range of generations G. Moreover, its implementation can be carried out by employing the standard, Metropolis Monte Carlo algorithm: no resorting to specially designed moves is necessary. In our approach, we envision every monomer as a hard sphere of diameter σ whereas the bonding between monomers is modeled by flexible threads of maximum extension $\Delta = \sigma(1 + \delta)$. The extension of the thread can be varied and offers one tunable parameter for the model. On the other hand, to test the sensitivity of the conformational properties of the dendrimers on the details of the microscopic interactions employed, we compare the results of the bead−thread model to those of the standard model of Murat and Grest.[14] We examine exclusively dendrimers with spacer length $P = 1$, and we adopt the notation G for the terminal generation and $g \leq G$ to denote internal generations within the dendrimer. The main results of our work read as follows: we find clear evidence of universality of the static conformational properties of the dendrimers at the mesoscopic level. When scaled with the radius of gyration, density profiles and form factors arising from different models practically collapse on one another. Moreover, we calculate the evolution of the scattering form factor with generation, finding a tendency of the molecules toward sphericity and compactness with growing G, in accordance with recent experimental results.[26] The distribution of end monomers is also broad, once again in agreement with recent SANS measurements.[27] Finally, the radius of gyration R_g does not scale with the number of monomers N as a simple power law for the whole range of N considered.

The rest of the paper is organized as follows. In section II, we discuss the models and the details of the simulation technique. In section III, we present and compare the results obtained from different models regarding the monomer and end-monomer density distributions for various generations. In section IV, we show the results for the form factors and compare them with experimental ones, demonstrating thereby the relevance of the proposed model for describing real dendrimers. Finally, in section V we summarize and conclude.

II. The Model and Simulation Details

A commonly used model for dendrimers is to treat the monomers (Kuhn segments) as bonded spherical beads, whereby the interaction between monomers is described by a pure repulsive Lennard-Jones-like potential and the bonds by the finite-extensible-nonlinear-elastic (FENE) potential.[14] This model will be denoted in the following as "model A". In detail, in model A the potential $U_{mm}(r)$ between nonbonded monomers is given by

$$U_{mm}(r) = \begin{cases} \phi_{LJ}(r) - \phi_{LJ}(r_c) & \text{for } r \leq r_c \\ 0 & \text{for } r > r_c \end{cases} \quad (1)$$

where $\phi_{LJ}(r)$ is the standard Lennard-Jones interaction

$$\phi_{LJ}(r) = 4\epsilon\left[\left(\frac{\sigma_{LJ}}{r}\right)^{12} - \left(\frac{\sigma_{LJ}}{r}\right)^{6}\right] \quad (2)$$

The cutoff distance r_c allows for the modeling of solvents of varying quality. The choice $r_c = 2^{1/6}\sigma_{LJ}$ renders the monomer−monomer interaction purely repulsive and thus suitable for an effective description of athermal solvents. Increasing r_c adds an attractive tail to the interaction. In this way, the value of the second virial coefficient B_2 of the interaction can be tuned, and the Θ ($B_2 = 0$) and poor ($B_2 < 0$) solvents can be incorporated into the model. Here we compare our results with those obtained by employing[22] $r_c = 2^{1/6}\sigma_{LJ}$ that models athermal solvents. Furthermore, bonded monomers are connected via a FENE potential U_{FENE}, acting in addition to U_{mm}:

$$U_{FENE}(r) = \begin{cases} -15\epsilon\left(\frac{R_0}{\sigma_{LJ}}\right)^2 \ln\left[1 - \left(\frac{r}{R_0}\right)^2\right] & \text{for } r \leq R_0 \\ \infty & \text{for } r > R_0 \end{cases} \quad (3)$$

where $R_0 = 1.5\sigma_{LJ}$ and $T = 1.2\epsilon/k_B$. The combination of the steric and FENE interactions comprises model A, which was originally introduced by Murat and Grest.[14] This model was also recently employed by Harreis et al.[22] in an analysis of the fluctuations of G4 dendrimers, and it was shown that it produces excellent agreement with SANS measurements for the form factor.

The essential features of model A are a strong repulsion between monomers and a maximum bond length. An even simpler model featuring the same characteristics is defined by a hard-sphere interaction $V_{HS}(r)$ that plays the role of $U_{mm}(r)$ and ideal "threads" with a maximum extension that connect the beads and

whose effect is given by the interaction potential $V_{bond}(r)$ below. Explicitly, we have

$$V_{HS}(r) = \begin{cases} \infty & \text{for } r/\sigma < 1 \\ 0 & \text{otherwise} \end{cases} \quad (4)$$

for nonbonded monomers and

$$V_{bond}(r) = \begin{cases} \infty & \text{for } r/\sigma < 1 \\ 0 & \text{for } 1 < r/\sigma < 1 + \delta \\ \infty & \text{for } r/\sigma > 1 + \delta \end{cases} \quad (5)$$

for bonded monomers; i.e., the hard spheres of diameter σ are connected by threads of contour length $\delta\sigma$. To avoid the occurrence of ghost chains during the simulations, δ has to be chosen smaller than $\sqrt{2} - 1 \cong 0.414$. This bead−thread model was employed in the recent work of Sheng et al.,[21] who examined the dependence of the radius of gyration of dendrimers on the spacer length and generation number, restricted to the case $\delta = 0.4$. No results for density distributions or form factors were examined, however. In what follows, this model will be denoted "model B".

In Monte Carlo simulations of model B, it is not necessary to calculate the potential energy or the forces; one only needs to check for overlaps of particles and whether the maximum bond length condition is fulfilled. Therefore, Monte Carlo simulations of this model are very fast, which is important due to the exponential growth of the number of monomers with the generation number. In the limit $\delta = 0$, model B reduces to tangent hard spheres, a model commonly used for simulations of polymers. Lue and Prausnitz[17] have also employed the tangent hard-spheres model to simulate dendrimers, with the difference that there the angle between two bonds at each branching site was fixed to 120°.

We simulated dendrimers of terminal generations $G = 4$ to $G = 9$ having the architecture sketched in Figure 1. The dendra emanate from two central trifunctional units glued together, and thereby the two central monomers comprise the zeroth-order generation, $g = 0$. In this architecture, the total number of monomers $N(g)$ up to the gth generation is given by

$$N(g) = (f - 1)[(f - 1)^{g+1} - 1] \quad (6)$$

where $f = 3$. The total degree of polymerization is $N = N(G)$. For $G \gg 1$, the ratio of the monomers at the terminal generation, $N_{end} = N(G) - N(G - 1) = (f - 1)^{G+1}$, obeys the relation $N/N_{end} \rightarrow 2$; thus, there are as many end monomers as in all previous generations.[28] This exponential growth of the number of monomers with G is a unique characteristic of the dendrimers and arises from their hierarchical, self-similar architecture. It immediately has as consequence that above a certain maximum generation no space is any more available to accommodate the self-avoiding monomers, and dendrimers cannot be grown any more.

To generate an initial configuration, a dendrimer of generation G is built of a dendrimer of generation $G - 1$ by trying to attach the additional end groups during a separate Monte Carlo simulation. To achieve this, for all monomers of the generation $G - 1$ that do not have end groups yet, we generate randomly two test monomers at a distance σ. These two test monomers are checked for overlap with each other and all other existing monomers. If no overlap occurs, the test monomers are accepted as end monomers, and subsequently they are allowed to move up to a maximum distance $(1 + \delta)\sigma$ from their parent monomer, according to eq 6. Otherwise, new positions for the test monomers are generated up to 100 times. This procedure is repeated during each MC step.

As an alternative way to produce the initial configuration, we also generate one of the two arms of the dendrimer randomly, which is subsequently duplicated and mirrored. These two arms are then pulled together in a separate MC simulation. To create the random arm, we use a recursive function that creates two new randomly oriented unit vectors to a given vector, i.e., the direction of the connection between the considered monomer and its origin monomer in the generation below. For these two new positions, overlaps are checked, and if they are accepted, the function calls itself for these two vectors until the requested generation number is reached. If after 10 000 test positions no two new vectors could be found, the recursion is aborted and started anew at the central monomer. This second method, though, yielded accepted configurations within feasible time scales only up to terminal generations $G = 7$; for higher G's the required time turns out to be prohibitively long. We have tested that the two methods of generating the initial configuration lead to identical conformational averages after the equilibration time, guaranteeing that the dendrimers have relaxed, and we are indeed sampling equilibrium configurations. We were not able to find any acceptable initial states for dendrimers larger than G9 employing spacer lengths $\delta = 0.05$ and 0.10. However, growth of a G10 dendrimer has been achieved with spacer lengths $\delta = 0.30$ and 0.40. Typically, after a phase of equilibration of 10^7 Monte Carlo steps, 10^8 (for G4) to 10^9 (for G9) MC steps were simulated, of which 4×10^5 to 4×10^6 configurations were used to calculate the statistical averages. To provide an additional check of the equilibration procedure, we increased the equilibration time by a factor 10, especially for the G8 and G9 dendrimers, finding no change in the resulting density profiles and sizes beyond the level of statistical noise. Moreover, since there is no energy to be monitored during equilibration in our model (pure hard-sphere interactions), we have monitored instead the growth of the radius of gyration during the process of adding end groups to generate dendrimer GN from an equilibrated dendrimer G$(N - 1)$. Throughout the process of adding the end groups, R_g grows monotonically. After all the end groups have been attached, R_g shows small variations well within the equilibration time, but after no more that 50 000 MC steps it saturates to its final value and only shows statistical noise variance around its average thereafter.

III. Density Distributions

In this section we present the results regarding the density distributions from MC simulations of model B with varying the spacer length δ and their comparisons with those from MC simulations of model A described above.[22]

Since our dendrimers lack a central monomer, we are led to consider the radial density distributions with

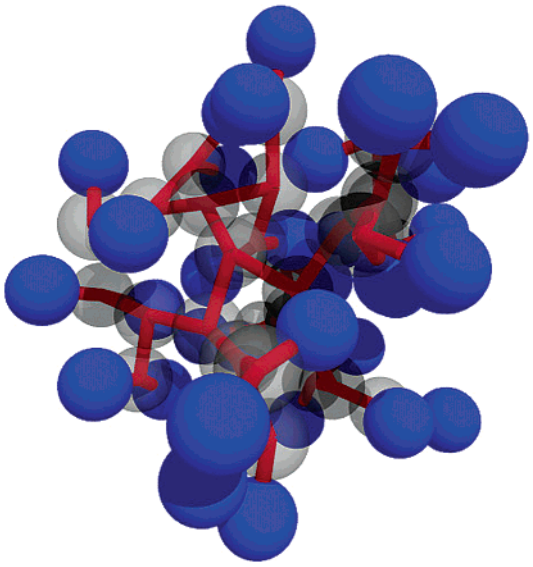

Figure 2. Simulation snapshot of a G4 dendrimer using model B with $\delta = 0.10$. The blue spheres of diameter σ denote the monomers of the end groups, while all other monomers are represented by semitransparent spheres. The bonds between the monomers are rendered as cylinders. The spread of the end monomers inside the dendrimer can be clearly discerned.

respect to their centers of mass instead. The latter is defined as

$$\rho(r) = \langle \sum_{i=1}^{N} \delta(\mathbf{r} - \mathbf{r}_i) \rangle \tag{7}$$

with N being the number of monomers comprising the dendrimer. Here, $\mathbf{r}$ and the coordinates of the monomers $\mathbf{r}_i = \mathbf{x}_i - \mathbf{x}_{CM}$ are measured with respect to the dendrimer's center of mass, whereby $\mathbf{x}_i$ are the coordinates in some fixed frame of reference and

$$\mathbf{x}_{CM} = \frac{1}{N} \sum_{i=1}^{N} \mathbf{x}_i \tag{8}$$

The process of taking configurational averages $\langle \cdots \rangle$ in eq 8 renders the density distribution radially symmetric. The same procedure can be applied to monomers belonging to any chosen generation g; of particular importance are those of the terminal generation $g = G$, and their density distribution will be denoted by $\rho_{end}(r)$.

Figure 2 shows a snapshot of a typical conformation of a G4 dendrimer, generated during the simulation employing model B. The results for the density distribution of the same are shown in Figure 3. The local minimum at $r = 0$ arises from the fact that the center of mass is located in the neighborhood of the midpoint between the two monomers making up the zeroth generation, and in this region few monomers can be found. Otherwise, we obtain typical dense-core profiles, with a narrow minimum after the first peak that comes about from the coordination between the $g = 0$ and $g = 1$ monomers. As can also be seen in Figure 2, end monomers are distributed throughout the dendrimer. A striking feature that emerges from the comparison between the density profiles of model B with two different spacer lengths ($\Delta \equiv \delta\sigma = 0.05\sigma$ and 0.10σ), as well as with the density profile from model A, is their strong insensitivity on the details of the microscopic

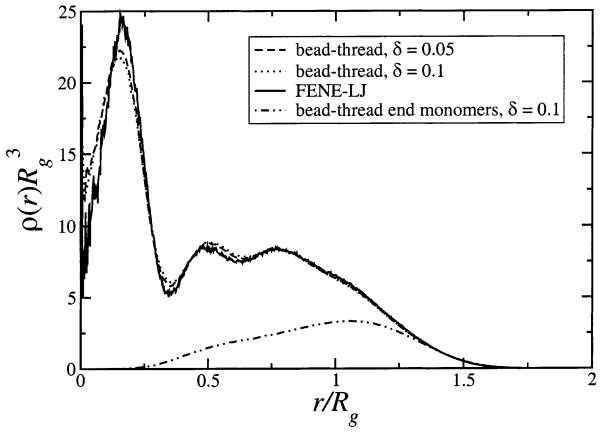

Figure 3. Radial density distribution of a G4 dendrimer with respect to the center of mass, normalized by the radius of gyration R_g. The solid line shows the result for model A (ref 22, courtesy of Holger Harreis); the dashed and dotted lines are the results for model B with the values $\delta = 0.05$ and 0.10. The density distribution of the end monomers for model B is shown as a dashed−dotted line.

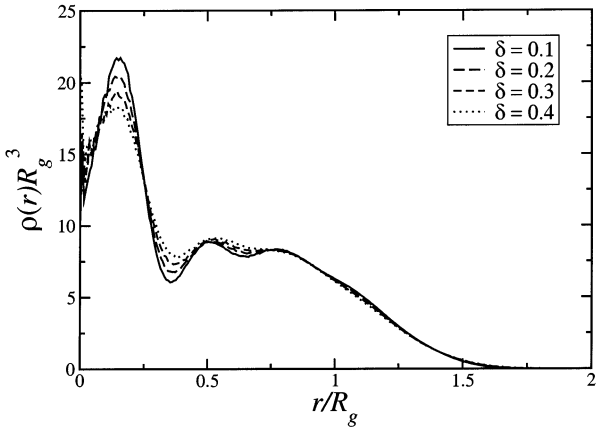

Figure 4. Radial density distribution of a G4 dendrimer for different values of δ. The dendrimer becomes larger for increasing δ, but R_g also increases, so that the extension of the density in terms of r/R_g remains constant. The peaks of the different shells are smeared out as δ increases because the connections become more loose.

interactions employed. When plotted by using σ or σ_{LJ} as units of length, the density profiles from the different models do differ. In particular, with increasing δ, the density spreads out to larger distances, and at the same time its height becomes smaller (so that its integral remains fixed to the number of monomers N). However, when the unit of length is rescaled to the gyration radius R_g, defined as

$$R_g = \sqrt{\frac{1}{N} \langle \sum_{i=1}^{N} (\mathbf{x}_i - \mathbf{x}_{CM})^2 \rangle} \tag{9}$$

all curves practically collapse on one another. The effect of changing the thread's contour length can still be discerned in the slightly weaker correlations present for larger δ, but it is rather small (see also Figure 4).

The procedure of using the radius of gyration as the length scale is not only the natural one for the coarse-grained description of the dendrimers, but it provides contact with experiments as well. Indeed, the microscopic parameter σ has no direct physical meaning, apart from the obvious requirement that it must be of

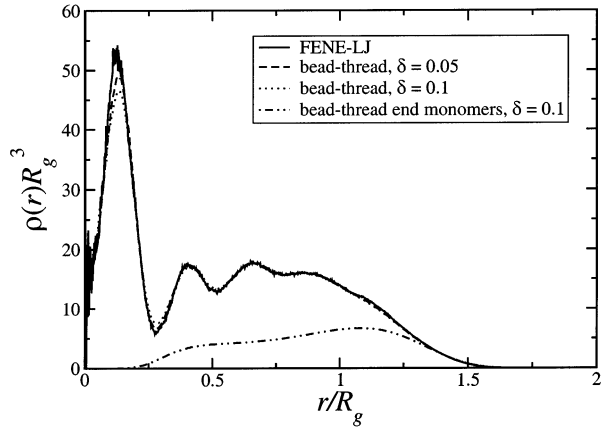

Figure 5. Same as Figure 3 but for a G5 dendrimer. The results for the LJ−FENE potential (solid line) are courtesy of Holger Harreis.

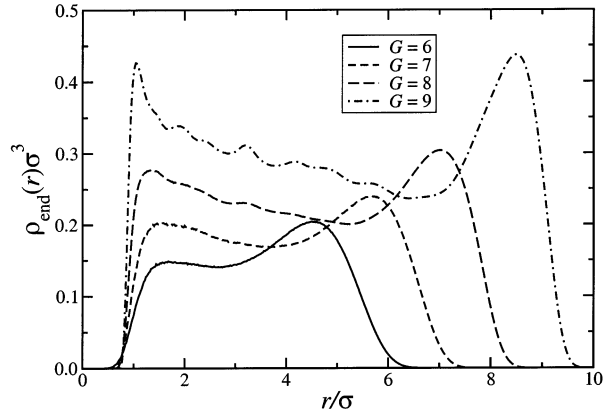

Figure 6. End-monomer density distributions for G6−G9 dendrimers, as obtained by the MC-simulation of model B with $\delta = 0.10$.

the order of the length of a Kuhn segment. In adopting a certain model to describe experimental data, the radius of gyration R_g which is measurable in small-angle scattering experiments provides the missing link between theory and experiment and allows for the assignment of a certain value to the parameter σ (see also ref 22). What we find here (and will be further confirmed in what follows) is that a broad one-parameter family of models, generated by varying the absolute value of a single microscopic scale, lead to practically identical results for the description of the dendrimers at the nanoscale.

This universality picture is further confirmed by the results for the G5 dendrimers, shown in Figure 5. Comparing with the density profile of the G4 dendrimers, three features show up: First, the correlation effects manifested in the peaks and troughs of the density profile become more pronounced. Second, a plateau of roughly constant density starts developing in the region $0.5 \lesssim r/R_g \lesssim 1.0$, but it should be emphasized that the height of this plateau is *not* constant but growing with G. Finally, the end-monomer distribution leaks more toward the central region of the molecule. We will return to the first two points shortly.

At this stage, it is interesting to monitor the development of the end-monomer distribution as a function of G for high generation numbers, G6 to G9. The result is shown in Figure 6. The outermost part of the dendrimer is populated by end monomers, but the converse is not true. With increasing G, the end monomers tend to distribute themselves within the molecule. There is a depression following the maximum at the edge of the molecule, caused by the fact that there the density profile of the $G - 1$ generation monomers displays its own local maximum. Some substructure is visible for $G = 8$ and $G = 9$ dendrimers. Strong back-folding of the dendra is taking place, a necessary mechanism for accommodating the increasingly large number of monomers, in agreement with findings in previous on- and off-lattice simulation studies involving a variety of model interparticle forces.[5,12−20] Preceding studies were limited to generation numbers $G \leq 7$, however. In this work, we demonstrate that the backfolding mechanism is also present for higher-generation dendrimers, but it can only be efficient if substantial stretching of the inner generations takes place. To visualize the very high degree of back-folding, we show in Figure 7 a simulation snapshot from a G6 dendrimer in which one selected, back-folded branch has been explicitly marked and in Figure 8 a snapshot of a G9 dendrimer and a view of the same configuration cut through the middle of the molecule.

By comparing Figures 2, 7, and 8, we first note that an increase in the terminal generation has the effect of turning the dendrimer more compact and its boundary sharper. Indeed, the loose outermost "blobs" that are visible for the G4 and G6 dendrimers have disappeared in the case of the G9 molecule. The distribution of end monomers in the whole of the molecule is evident. In the case of the G9 dendrimer, a very interesting feature emerges, namely the following: since the number of terminal monomers to be accommodated is becoming exceedingly high, the corresponding voids have to be created at some other place in the molecule, in particular in its interior. Thereby, the chains building the lower generations (up to $g = 4$) stretch and open up. The end monomers are now folding back into precisely the voids created by this stretching, as can be seen also by comparing the terminal generation and total density profiles in Figures 6 and 9. There is strong localization of the low-generation monomers, and the dendritic structure up to $g = 4$ becomes clearly visible. This should be compared with the snapshot of a dendrimer of *terminal* generation 4 in Figure 2. If the bonds were omitted there, it would be hard to say that the spheres belong to a dendrimer, whereas in Figure 8 the dendritic architecture of the lowest generations is immediately recognizable and has a clear similarity with the "flattened out", rigid chemical structure shown in Figure 1.

These features can be quantified by looking now at the total density profiles of the dendrimers, shown in Figure 9. With increasing G, strong peaks develop for the first few generation, indicating the strong localization of the monomers belonging to those and the stretching of the inner parts of the arms. This finding is in agreement with the recent theoretical results of Timoshenko et al.,[29] who considered a model of beads connected by harmonic springs. They found that the innermost springs connecting monomers are the most extended, with the degree of stretching decreasing as one moves along the terminal bead along a dendrimer's branch. In comparing the locations of the weak local maxima of the end-monomer distribution for G9, shown in Figure 6 with the total density profile in Figure 9, we see that the end monomers that fold back into the inner part of the molecule are to be found in the void regions created by the strongly stretched first few

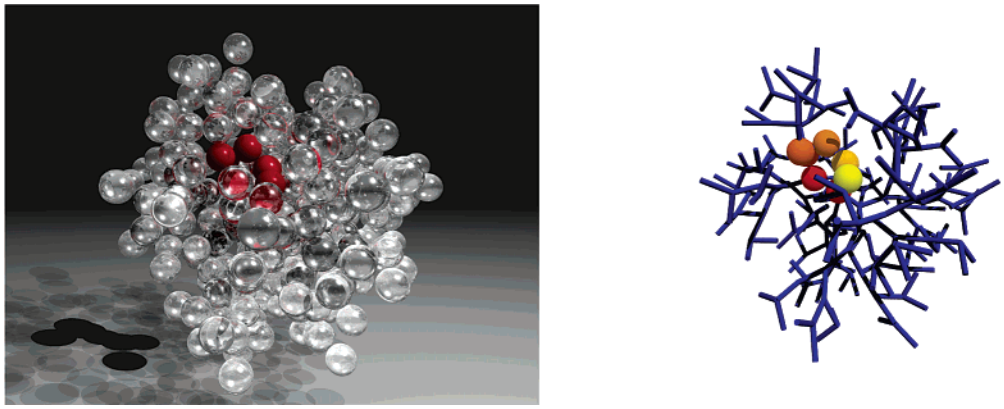

Figure 7. Simulation snapshot of a G6 dendrimer obtained by employing model B with $\delta = 0.10$. The left panel shows all monomers rendered as spheres of diameter σ. A single, back-folded branch has been selected and colored red, whereas all other monomers are rendered as glass spheres. The shadowing assists in demonstrating the back-folding of the branch within the body of the dendrimer. Right panel: here only the monomers of the back-folded branch are shown as spheres, and they are color-coded as follows: the end monomer is colored yellow, and it is situated within the dendrimer. Starting from this, a path leads to one of the two innermost monomers, colored red. Increasing intensity of red denotes approaching of the aforementioned central monomer. All other monomers are omitted for clarity, but the bonds are rendered as cylinders.

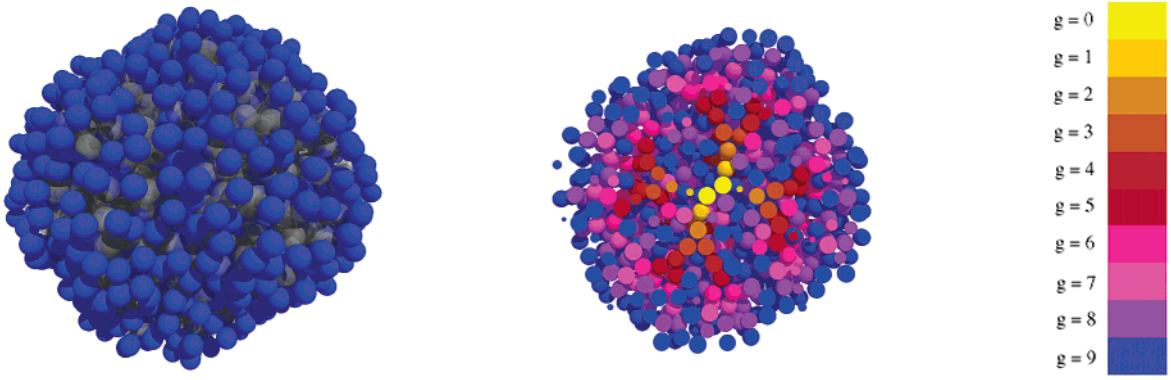

Figure 8. Simulation snapshot of a G9 dendrimer obtained by employing model B with $\delta = 0.10$. The left panel shows all monomers rendered as spheres of diameter σ, with those belonging to the end generation colored blue and all other rendered as semitransparent spheres of diameter σ. The outer surface is covered exclusively by $g = 9$ monomers, but there are also many end monomers within the dendrimer that are somewhat obscured by the high concentration of semitransparent spheres. Right panel: a cut through the middle of the configuration on the left, showing the coordination of the monomers belonging to various generations within the dendrimer. The generations are color-coded as indicated in the color bar on the right.

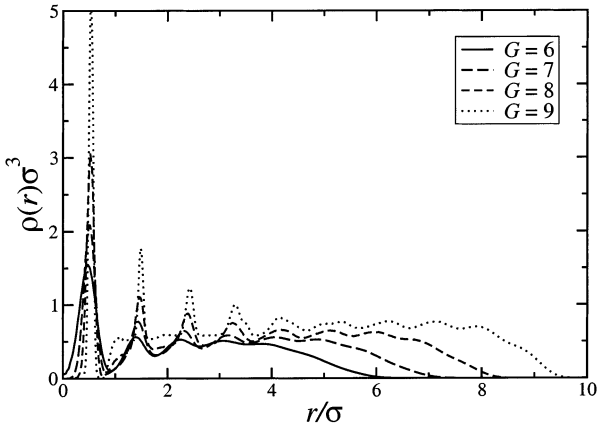

Figure 9. Density profiles for G6−G9 dendrimers obtained from model B with $\delta = 0.10$. Here, the bead diameter σ is used as the unit of length.

generations. These form a rigid structure, witnessed by the strong coordination peaks of the total density profiles in Figure 9. Additionally, we remark that the density profiles at $r = 0$ decrease to zero value upon increasing G. This implies that the center of mass becomes more and more sharply localized at the midpoint between the two beads of the zeroth generation as G increases, where no monomers are ever found. For lower values of G, the fluctuations of the molecule can displace the center of mass considerably and bring it occasionally in coincidence with the position of one of the central monomers, giving rise to the nonzero value of $\rho(r = 0)$. We draw the conclusion that dendrimers with $G \geq 6$ possess a rigid, nonfluctuating core consisting of the stretched first few generations and in those all (weak) fluctuations take place at the outermost part of the molecule.

Another question that has caused quite some controversy in the literature is that of the scaling of the gyration radius R_g with the number of monomers N. Lescanec and Muthukumar[5] found in their pioneering simulation work $R_g \sim N^{0.22\pm0.02}$, but some doubts regarding the equilibrated character of their configurations remained.[14] Murat and Grest,[14] on the other hand, report a scaling relation of the form $R_g \sim N^{1/3}$, indicating that dendrimers are compact structures with a constant average density within their volume. Since then, there have been various claims both in favor of the $\sim N^{1/3}$ law[10,12,20,24] and in favor of a $\sim N^{1/5}$ dependence.[16,21] Sheng et al.,[21] who employed the same model as we do for the special case $\delta = 0.40$, offered an explanation for these discrepancies. They found that when R_g is considered as a function of N for fixed spacer length P (the

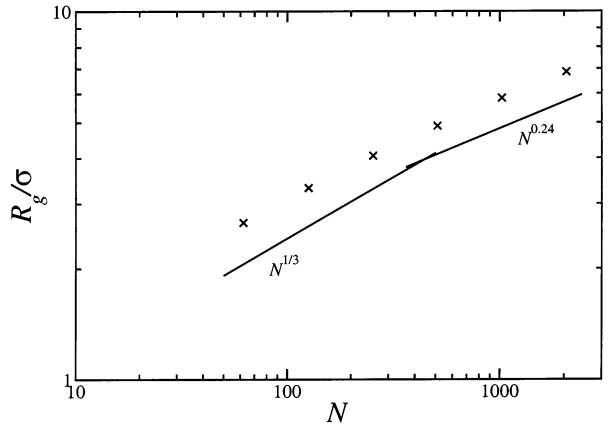

Figure 10. Double-logarithmic plot of the radius of gyration R_g against the number of monomers N of the dendrimers. The change in N is caused by an increase of G, and the results shown are for $G = 4$, 5, 6, 7, 8, and 9. It can be seen that the results for large N can be fitted by a power law $R_g \sim N^x$ with $x = 0.24$ and not by $R_g \sim N^{1/3}$. The error bars on the data are of the order of $10^{-3}\sigma$.

monomer number N changing through a change of the final generation G), then a scaling $R_g \sim N^{1/3}$ obtains. If one now keeps the generation number G fixed and varies N through a change of the spacer length, a different scaling, $R_g \sim N^{3/5}$, identical to the behavior of linear polymers obtains. But if one wants to describe all dependencies of R_g in a single scaling law, then the correct dependence is indeed $R_g \sim (PG)^{2/5}N^{1/5}$, as conjectured by Chen and Cui.[16] In all preceding studies, typical generations range from G3 to G7, and monomer numbers lie in the domain $10 \lesssim N \lesssim 1000$.

We have also examined the N dependence of R_g in our study, in which however we have a fixed spacer number $P = 1$ and thus we can vary N only through a variation of the generation number G. The results are shown in Figure 10. It is clear that a single power-law of the type $R_g \sim N^{1/3}$ does not describe the R_g dependence in the whole range of N considered. Even at small generation dendrimers, G4 to G7, there are slight deviations from this law, which become strong for the higher generations, G7 to G9. For the latter case, a dependence of the form $R_g \sim N^{0.24}$ appears to hold. Taking into account the finding of Sheng et al.[21] that the correct scaling has the form $R_g \sim (PG)^{2/5}N^{1/5}$ and that in our model $P = 1$ and $G \sim \ln N$, we see that rather a dependence of the type $R_g \sim (\ln N)^{0.4}N^{0.2}$ obtains. In the N domain corresponding to G7−G9 dendrimers, this dependence strongly resembles a $\sim N^{0.24}$ law. Thus, our finding should not be interpreted as a universal law but rather as a local fit of the results in the region $400 \lesssim N \lesssim 2000$. Our results are in agreement with the original prediction of an exponent $x = 0.22 \pm 0.02$ of Lescanec and Muthukumar[5] within error bars and close to the exponent $^1/_5$ of Chen and Cui[16] and Sheng et al.[21] Giupponi and Buzza[24] also reported deviations from the $^1/_3$ exponent in their lattice model; however, these were much weaker than the ones we find here. The explanation for the deviation from the "compact sphere" exponent $^1/_3$ can be found in Figure 9, showing the density profiles of the dendrimers. It can be seen that there exists a large plateau in the monomer profiles, in which the density is roughly constant. Were this constant value to be also independent from G, this would lead to the conclusion of a $R_G \sim N^{1/3}$ dependence. We notice, however, that by increasing G the height of the plateau itself increases. Thus, if we envision the dendrimers as homogeneous spheres to a first approximation, we see that the density of these spheres grows with G, and thus the $N(G)$ monomers are packed more and more densely. This causes the exponent to be significantly smaller than $^1/_3$ and having the apparent value 0.24. It should also be noted that the deviation from the $R_G \sim N^{1/3}$ dependence is connected with the stretching of the innermost generations for the G7, G8, and G9 dendrimers, in conjunction with the short-spacer condition, $P = 1$, employed in our study. The innermost generations for these dendrimers cannot be described as flexible chains anymore, and hence a universal scaling law cannot be valid.

The existence of the density plateau is in agreement with the result of Murat and Grest,[14] but our findings are at odds with their claim that the value of the density at this plateau is independent of the generation number. On the other hand, our simulation is in agreement with two recent scattering studies. A clear deviation from the $N^{1/3}$ law for dendrimers with $4 \le G \le 8$ has been seen in the SAXS experiments of Rathgeber et al.[26] An analysis of the results reported there on the basis of a Guinier fit of the scattering intensities (Table 1 and Figure 6 of ref 26) yields the law $R_g \sim N^{0.24}$, in precise agreement with our results. The authors of ref 26 also argued on the grounds for this slower increase of R_g along the same lines as we do.[30] Moreover, Mallamace et al.[31] report for high-generation dendrimers a scaling exponent $R_g \sim N^{0.21}$ from a Guinier fit of SAXS measurements, again close the value 0.24 we obtained in our simulations but very different from the oft-proposed value 0.33.

IV. Form Factors

The form factor $F(q)$ depending on the wavenumber q is a very useful quantity as it contains information on the size and shape of the molecules on one hand and it provides a direct link with experiments on the other. Indeed, when scattering (light, X-rays, or neutrons) from dilute suspensions, the coherent scattering intensity $I_S(q)$ at scattering wavevector q is proportional to the form factor $F(q)$.[32,33] The latter is defined as[34−36]

$$F(q) = 1 + \frac{1}{N}\left\langle \sum_{i=1}^{N}\sum_{j\neq i}^{N} \exp[-i\mathbf{q}\cdot(\mathbf{r}_i - \mathbf{r}_j)] \right\rangle \qquad (10)$$

with the instantaneous positions $\mathbf{r}_{i,j}$ of the ith and jth monomer, the scattering wavevector $\mathbf{q}$ and the average over all conformations, $\langle\cdots\rangle$. The behavior of $F(q)$ at small values of the wavenumber determines the gyration radius, since it holds[35]

$$F(q) \cong N\left[1 - \frac{(qR_g)^2}{3}\right] \quad (qR_g \ll 1) \qquad (11)$$

Very good agreement between the experimentally determined form factor for G4 dendrimers, and the one obtained from simulations of model A has been found in ref 22. The corresponding result for model B is shown in Figure 11. The simulation data (full line) are within the error bars of the experimental data obtained by SANS.[32,33]

Further, as can be seen in Figure 12, the form factor is nearly independent from microscopic details like the thread contour length δ or even the model type itself (A, B), when q is scaled with the radius of gyration R_g.

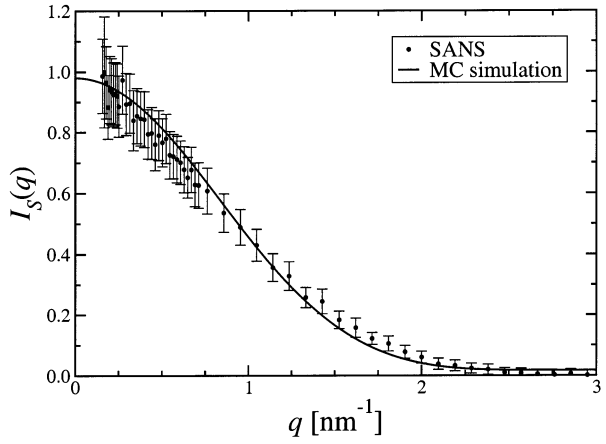

Figure 11. Total scattering intensity $I_S(q)$ from a dilute solution of G4 dendrimers. The circles are SANS data from ref 33. The solid line is obtained from the simulation form factor of model B with $\delta = 0.10$. The simulation yields $F(q)$ as a function of $q\sigma$. The value of σ is determined so as to obtain the experimentally measured radius of gyration, $R_g = 1.489$ nm in this case, and the horizontal axis is appropriately rescaled. The vertical axis can be rescaled freely, since it involves the contrast factor between monomers and solvent which is an arbitrary parameter in a coarse-grained simulation.

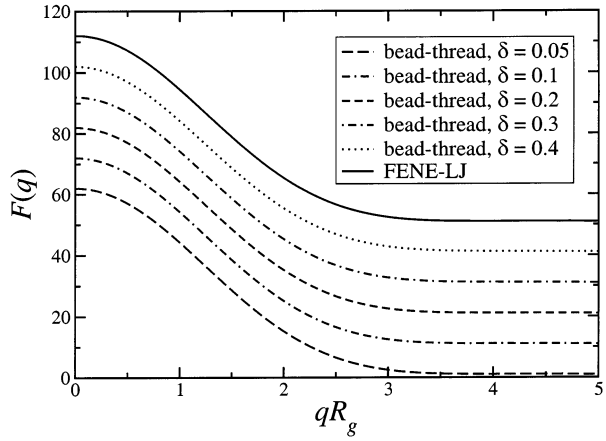

Figure 12. Form factors of G4 dendrimers (solid line: model A, ref 22; dashed lines: model B with $\delta/\sigma = 0.05$, 0.10, 0.20, 0.30, 0.40). For clarity, the curves have been shifted upward in amounts of 10 (from bottom to top); otherwise, they all collapse and they become indistinguishable.

This feature is similar to the one already discussed regarding the density profiles, but it is even stronger for the form factor because the various $F(q)$ curves indeed collapse on one another. Therefore, the form factor alone, and its comparison to scattering data, is not sufficient to decide which model is most suitable to describe the given dendrimers.

Finally, in Figure 13 we show the form factors of G4−G9 dendrimers on a double-logarithmic scale. With increasing generation number, an oscillatory structure in the domain $qR_g \gtrsim 3$ shows up, signaling the fact that the dendrimers develop sharper boundaries. The oscillations first appear for generation numbers exceeding $G = 5$, in agreement with other simulation studies.[20,24,37] The form factor for $G = 9$ has an envelope that scales as $\sim q^{-4}$ at high values of the wavenumber, which represents Porod's law for scattering from a compact sphere.[31] The shapes of the curves, their evolution with G, and the locations of the minima are additionally in very good agreement with experimental scattering

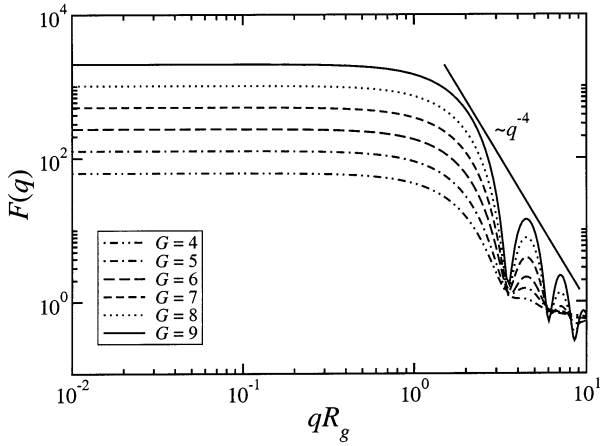

Figure 13. Double-logarithmic plot of the form factors for dendrimers G4−G9 obtained by the simulation of model B with $\delta = 0.10$. The straight solid line represents Porod's law, $F(q) \sim q^{-4}$.

curves from dendrimers of varying generation numbers.[26,31,38,39] This amply demonstrates the ability of the present model to describe real dendrimers.

V. Summary and Concluding Remarks

We have introduced a "minimal" model to describe dendrimers of various generations. Our approach takes into account the connectivity and steric interactions of self-avoiding dendrimers in the very simple way, by viewing the monomers as hard spheres connected by ideal threads that have a maximum possible extension. We focused on dendrimers with spacer length $P = 1$ and on athermal solvents in this study, but the generalization to arbitrary P's and to solvents of varying quality is straightforward. One can introduce a tunable effective attraction of varying shape, depth, and range in order to model solvents of decreasing quality. We have shown that the dendrimers are a distinct class of polymeric colloids, possessing a density profile that features a broad plateau of constant density. This makes them clearly distinct from other branched polymeric entities, such as star polymers for which a density profile $\rho(r) \sim r^{-4/3}$ holds,[40] or star-branched polyelectrolytes, in which case a dependence of the form $\rho(r) \sim r^{-2}$ obtains.[41,42] In addition, the height of this plateau was found to be generation-dependent, a feature that causes the size of the dendrimers to grow with the number of monomers slower than the inverse-third power of the latter, as has been observed experimentally. The form factors obtained are also in very good agreement with experiments.

An important property of the models we considered is a strong insensitivity of the results on the details of the microscopic model. This holds both for the bead−thread model, in which the contour length was varied by a factor 8 (from 0.05 to 0.40), and for the Lennard-Jones−FENE potential. When lengths are scaled with the radius of gyration of the molecule, results practically collapse on master curves. This has the implication that one cannot determine on the basis of comparisons with scattering data from dilute solutions alone which model is the most realistic for the system at hand. On the other hand, a quantity that most certainly does depend on the model details is the effective interaction (potential of mean force) between two dendrimers. Preliminary calculations indicate[43] that the shorter the contour length, the more repulsive the resulting effective interaction.

Since the latter determines the scattering curves from concentrated solutions, through the structure factor $S(q)$ of the system, we argue that accurate experiments at finite concentrations are of particular importance. The simplicity of the microscopic model put forward in this work renders the calculation of the effective interaction straightforward in a Monte Carlo simulation, and our preliminary results indicate that the model is capable of explaining scattering profiles from concentrated dendrimer solutions. The presentation of these findings will be the subject of a future publication.

Acknowledgment. We thank Holger Harreis for providing simulation results for model A and helpful discussions and Matthias Ballauff for helpful discussions. This work has been supported by the Deutsche Forschungsgemeinschaft (DFG).

References and Notes

(1) Newcome, G. R.; Moorefield, C. N.; Vögtle, F. *Dendrimers and Dendrons*; Wiley WCH: Weinheim, Germany, 2001.
(2) Trollsås, M.; Atthof, B.; Würsch, A.; Hedrick, J. L.; Pople, J. A.; Gast, A. P. *Macromolecules* **2000**, *33*, 6423.
(3) Tomalia, D. A., Fréchet, J. M. J., Eds.; *Dendrimers and Other Dendritic Polymers*; Wiley: Chichester, 2002.
(4) De Gennes, P. G.; Hervet, H. *J. Phys., Lett.* **1983**, *44*, L351.
(5) Lescanec, R. L.; Muthukumar, M. *Macromolecules* **1990**, *23*, 2280.
(6) Boris, D.; Rubinstein, M. *Macromolecules* **1996**, *29*, 7251.
(7) Zook, T. C.; Pickett, G. T. *Phys. Rev. Lett.* **2003**, *90*, 105502.
(8) Milner, S. T.; Witten, T. A.; Cates, M. E. *Macromolecules* **1988**, *21*, 2610.
(9) Naylor, A. M.; Goddard, W. A.; Kiefer, G. E.; Tomalia, A. D. *J. Am. Chem. Soc.* **1989**, *111*, 2339.
(10) Scherrenberg, R.; Coussens, B.; van Vliet, P.; Edouard, G.; Brackman, J.; de Brabander, F.; Mortensen, K. *Macromolecules* **1998**, *31*, 45.
(11) Cavallo, L.; Fraternali, F. *Chem.—Eur. J.* **1998**, *4*, 927.
(12) Zacharopoulos, N.; Economou, I. G. *Macromolecules* **2002**, *35*, 1814.
(13) Mansfield, M. L.; Klushin, I. *Macromolecules* **1993**, *26*, 4262.
(14) Murat, M.; Grest, G. S. *Macromolecules* **1996**, *29*, 1278.
(15) Carl, W. *J. Chem. Soc., Faraday Trans.* **1996**, *92*, 4151−4154.
(16) Chen, Z. Y.; Cui, S.-M. *Macromolecules* **1996**, *29*, 7943.
(17) Lue, L.; Prausnitz, J. M. *Macromolecules* **1997**, *30*, 6650.
(18) Lue, L. *Macromolecules* **2000**, *33*, 2266.
(19) Lyulin, A. V.; Davies, G. R.; Adolf, D. B. *Macromolecules* **2000**, *33*, 3294.
(20) Karatasos, K.; Adolf, D. B.; Davies, G. R. *J. Chem. Phys.* **2001**, *115*, 5310.
(21) Sheng, Y.-J.; S. Jiang, S.; Tsao, H.-K. *Macromolecules* **2002**, *35*, 7865.
(22) Harreis, H. M.; Likos, C. N.; Ballauff, M. *J. Chem. Phys.* **2003**, *118*, 1979.
(23) Wallace, E. J.; Buzza, D. M. A.; Read, D. J. *Macromolecules* **2001**, *34*, 7140.
(24) Giupponi, G.; Buzza, D. M. A. *Macromolecules* **2002**, *35*, 9799.
(25) Mansfield, M. L.; Jeong, M. *Macromolecules* **2002**, *35*, 9794.
(26) Rathgeber, S.; Monkenbusch, M.; Kreitschmann, M.; Urban, V.; Brulet, A. *J. Chem. Phys.* **2002**, *117*, 4047.
(27) Rosenfeldt, S.; Dingenouts, N.; Ballauff, M.; Werner, N.; Vögtle, F.; Lindner, P. *Macromolecules* **2002**, *35*, 8098.
(28) A slightly different architecture is often employed in the literature, in which $f = 3$ dendra emerge from a single central monomer. In this case, the group of the first four monomers comprises the zeroth generation, and eq 7 must be replaced with the expression $N(g) = 1 + f[(f-1)^{g+1} - 1]$. However, none of the conclusions in this work are essentially affected by this modification in the architecture.
(29) Timoshenko, E. G.; Kuznetsov, Yu. A.; Connolly, R. *J. Chem. Phys.* **2002**, *117*, 9050.
(30) The dendrimers of ref 26 had again a slightly different architecture than ours, for which the number of monomers $M(g)$ up to generation g is given by $M(g) = (f-1)^{g+3} - f$. Comparing this relation with eq 7, we find $N(g) = M(g-1) + 1 \cong M(g-1)$ since $M(g-1) \gg 1$. Thus our simulation results for dendrimers of generation G correspond, in the notation of ref 26, to experimental ones for dendrimers of generation $G-1$.
(31) Mallamace, F.; Canetta, E.; Lombardo, D.; Mazzaglia, A.; Romeo, A.; Monsù Scolaro, L.; Maino, G. *Physica A* **2002**, *304*, 235.
(32) Pötschke, D.; Ballauff, M.; Lindner, P.; Fischer, M.; Vögtle, F. *Macromol. Chem. Phys.* **2000**, *201*, 330.
(33) Rosenfeldt, S.; Dingenouts, N.; Ballauff, M.; Lindner, P.; Likos, C. N.; Werner, N.; Vögtle, F. *Macromol. Chem. Phys.* **2002**, *203*, 1995.
(34) Hansen, J. P.; MacDonald, I. R. *Theory of Simple Liquids*, 2nd ed.; Academic: New York, 1986.
(35) Higgins, J. S.; Benoît, H. C. *Polymers and Neutron Scattering*; Clarendon Press: Oxford, 1994.
(36) Klein, R.; D'Aguanno, B. In *Light Scattering: Principles and Development*; Brown, W., Ed.; Clarendon Press: Oxford, 1996.
(37) Mansfield, M. L. *Macromolecules* **2000**, *33*, 8043.
(38) Prosa, T. J.; Bauer, B. J.; Amis, E. J. *Macromolecules* **2001**, *34*, 4897.
(39) Nisato, G.; Ivkov, R.; Amis, E. J. *Macromolecules* **2000**, *33*, 4172.
(40) Grest, G. S.; Fetters, L. J.; Huang, J. S.; Richter, D. *Adv. Phys. Chem.* **1996**, *XCIV*, 67.
(41) Guenoun, P.; Muller, F.; Delsanti, M.; Auvray, L.; Chen, Y. J.; Mays, J. W.; Tirell, M. *Phys. Rev. Lett.* **1998**, *81*, 3872.
(42) Jusufi, A.; Likos, C. N.; Löwen, H. *Phys. Rev. Lett.* **2002**, *88*, 018301; *J. Chem. Phys.* **2002**, *116*, 11011.
(43) Götze, I. O.; Harreis, H. M.; Likos, C. N., manuscript in preparation.

MA030137K